Research Square

Preprints are preliminary reports that have not undergone peer review.
They should not be considered conclusive, used to inform clinical practice,
or referenced by the media as validated information.

Identification of Performance-Related Movement Patterns During the Tennis Forehand High-Ball Stroke Using Principal Component Analysis

Jiujiang Liu
Yanshan University
Yang Sun
Yanshan University
Hanbing Wu
Yanshan University
Zihao Lu
Yanshan University
Danyang Kou
Yanshan University
Yuling Fang
Yanshan University
Jingwen Gao
Yanshan University
Gangzheng Yi
Yanshan University
Yuan Gao
gaoyuan1107@ysu.edu.cn
Yanshan University

Research Article

Keywords: Tennis forehand high-ball stroke, Principal component analysis, Waveform reconstruction, Racket-head speed

Posted Date: November 17th, 2026

DOI: https://doi.org/10.21203/rs.3.rs-11248833/v1

License: This work is licensed under a Creative Commons Attribution 4.0 International License.
Read Full License

Additional Declarations: No competing interests reported.

Identification of Performance-Related Movement Patterns During the Tennis Forehand High-Ball Stroke Using Principal Component Analysis

Jiujiang Liu [a], Yang Sun [b], Hanbing Wu [a], Zihao Lu [a], Danyang Kou [a], Yuling Fang [a], Jingwen Gao [a], Gangzheng Yi [a], Yuan Gao [a]*

[a]School of Physical Education, Yanshan University, Qinhuangdao 066004, China

[b]School of Mechanical Engineering, Yanshan University, Qinhuangdao 066004, China

* Correspondence: gaoyuan1107@ysu.edu.cn (Yuan Gao)

Abstract

Whole-body movement patterns associated with performance during the tennis forehand high-ball stroke remain insufficiently characterized. This study used principal component analysis (PCA) and waveform reconstruction to identify kinematic patterns associated with peak racket-head speed and acceleration. Twenty-eight male recreational tennis players with formal training performed closed-stance forehand high-ball strokes while three-dimensional kinematics were recorded. Forty-two kinematic variables were time-normalised across the backswing, forward swing, and follow-through phases and analysed using PCA. Retained component scores were correlated with peak racket-head speed and acceleration using Pearson correlation analysis. The first 13 components explained 80.43% of the total variance. The fifth principal component (PC5) was positively correlated with peak racket-head speed ($r = 0.553$, $p = 0.002$) and acceleration ($r = 0.485$, $p = 0.009$). Waveforms reconstructed at three standard deviations above and below the mean PC5 score associated higher performance with earlier thoracic rotation during the backswing, greater hip and shoulder abduction during the forward swing, and more stable pelvic and thoracic alignment during the follow-through. These exploratory findings identify a whole-body kinematic pattern associated with racket performance and suggest movement features for further investigation in tennis technique training.

Keywords: Tennis forehand high-ball stroke; Principal component analysis; Waveform reconstruction; Racket-head speed

Introduction

In recent years, the evolution of modern tennis tactics has led to baseline rallies dominated by topspin groundstrokes. Previous studies have shown that contemporary players increasingly employ topspin to improve shot consistency while maintaining stroke quality (Huang and Gao, 2023; Lambrich and Muehlbauer, 2023; Genevois et al., 2020). Greater topspin substantially alters ball trajectory and rebound behavior, producing a higher and faster post-bounce trajectory (Lambrich and Muehlbauer, 2023; Biber et al., 2023) and consequently increasing the frequency of high-ball situations during match play. To respond effectively, players must strike the ball at a higher contact point, placing greater demands on temporal perception, body positioning, and whole-body movement control.

Among the movement strategies used to manage high-bouncing balls, the closed stance is frequently adopted because it provides a stable anterior–posterior base of support, facilitates vertical body alignment, and promotes efficient force transmission throughout the kinetic chain (Caprioli et al., 2025; Elliott et al., 2009). Compared with open or semi-open stances, the closed stance requires greater lower-limb stability, more precise control of forward center-of-mass progression, and enhanced pelvis–trunk separation (Martin et al., 2020). Consequently, the forehand high-ball stroke should not be regarded as merely a variation of the conventional forehand; rather, it represents a more demanding motor task requiring highly coordinated control of multiple body segments.

Efficient execution of the tennis forehand relies on the coordinated transfer of mechanical energy through the proximal-to-distal kinetic chain, from the lower extremities to the trunk and upper limb (Elliott, 2006; Huang and Gao, 2023). During high-level stroke production, joint angular velocity and acceleration typically increase sequentially from proximal to distal segments, reflecting efficient generation and transfer of mechanical energy (van Trigt et al., 2025). However, this proximal-to-distal sequencing is observed across players of different skill levels. Therefore, analysing movement timing alone is insufficient to explain why some players produce superior stroke performance. Instead, performance differences are more likely to arise from subtle variations in inter-segmental coordination, movement organization, and the regulation of biomechanical degrees of freedom (Gorce and Jacquier-Bret, 2024).

Principal component analysis (PCA) has become an established approach for investigating complex human movement by reducing high-dimensional kinematic data into a limited number of orthogonal movement patterns that capture the dominant sources of movement variability (Federolf, 2016; Gløersen et al., 2018). When combined with waveform reconstruction, PCA not only quantifies coordinated variations across multiple joints but also reconstructs representative movement patterns, providing an intuitive interpretation of the biomechanical characteristics associated with different performance levels (Deluzio and Astephen, 2007). Consequently, this approach offers a powerful framework for examining whole-body coordination beyond conventional joint-by-joint analyses.

Therefore, the present study combined principal component analysis with waveform reconstruction to identify the movement patterns associated with performance during the tennis forehand high-ball stroke. Specifically, we aimed to investigate how kinetic-chain sequencing, inter-segmental coordination, and degrees-of-freedom control contribute to stroke performance, thereby providing biomechanical evidence to support technique optimization and training interventions.

1. Methods

1.1 Participants

Participants were recruited from local universities. An a priori sample size analysis was performed using G*Power (version 3.1.9.7; Heinrich Heine University, Düsseldorf, Germany). Assuming a correlation effect size of 0.50, a significance level of 0.05, and a statistical power of 0.75, the minimum required sample size was estimated to be 26 participants. To account for potential data loss, 30 participants were initially recruited. Following data quality screening, two datasets were excluded because of incomplete or invalid recordings, resulting in a final sample of 28 participants.

All participants were male recreational tennis players with formal tennis training and were able to perform the forehand high-ball stroke proficiently. Eligibility criteria included: age between 18 and 25 years; a minimum of two years of systematic tennis training; the ability to execute the forehand high-ball stroke consistently; and no musculoskeletal injury affecting performance at the time of testing. Participants were excluded if they had a history of neuromuscular disorders, had undergone surgery or

structured rehabilitation within the previous six months, had performed vigorous exercise within 48 hours before testing, or failed to complete the experimental protocol or produced incomplete kinematic data.

Of the 28 participants, two were left-handed and 26 were right-handed. Participant characteristics are presented in Table 1.

Before testing, all participants provided written informed consent after receiving an explanation of the study procedures, risks, and objectives. As no applicable local ethics committee was available, the study was approved by the Medical Ethics Committee of Qinhuangdao Hospital, Peking University Third Hospital (Approval No. 2026Y005). All procedures complied with the Declaration of Helsinki.

Table 1. Participant characteristics (mean ± SD).

Variable	Value
Sample size, *n*	28
Age (years)	21.18 ± 1.47
Height (m)	1.79 ± 0.05
Body mass (kg)	73.75 ± 9.33
BMI ($kg \cdot m^{-2}$)	22.85 ± 2.74
Tennis training experience (years)	3.93 ± 1.25

1.2 Experimental Protocol and Data Collection

1.2.1 Experimental protocol

After providing written informed consent, participants changed into tight-fitting sportswear and completed a standardized warm-up consisting of 5–10 min of light jogging followed by dynamic stretching. Three-dimensional kinematic data were collected using an eight-camera Qualisys motion capture system (Qualisys AB, Gothenburg, Sweden) operating at 200 Hz.

A full-body marker set consisting of 55 retroreflective markers was attached according to the CAST Full-body model to establish anatomical coordinate systems using static calibration and cluster-based marker tracking (Cappozzo et al., 1995) (Figure 1). To quantify racket kinematics, six additional markers were attached to the racket to create a rigid-body model. A single reflective marker was attached to the underside of the tennis ball to identify the instant of ball–racket contact (Figure 1). All markers were placed by the same experienced investigator following standardized

anatomical landmark definitions to ensure consistency across participants.



Figure 1. Reflective marker placement for the participant, racket, and target ball.

Following marker placement, a static calibration trial was collected with participants standing in the anatomical position with both arms elevated horizontally. Participants were then familiarized with the testing procedure and allowed to perform practice trials until comfortable with the task. The position of the suspended ball was individually adjusted to match each participant's preferred contact height. Subsequently, each participant performed at least five maximal-effort forehand high-ball strokes, with verbal encouragement provided to ensure consistent performance throughout testing.

1.2.2 Experimental task

The experimental task consisted of a closed-stance forehand high-ball stroke. Participants initiated each trial with a split step from a designated starting position before stepping onto the force platform with the racket-side foot followed by the contralateral foot. After establishing a stable stance, participants executed the stroke at a fixed ball positioned above shoulder height and completed the movement with a natural follow-through before returning to the starting position for the next trial.

A closed-stance forehand high-ball stroke was operationally defined as a forehand stroke performed with the feet positioned in an anterior–posterior alignment, the trunk

oriented side-on to the direction of the incoming ball, and ball contact occurring above shoulder height. The movement comprised coordinated lower-limb propulsion, pelvis and trunk rotation, and upper-limb acceleration, generating an efficient proximal-to-distal kinetic chain for racket acceleration.

1.2.3 Movement phase definition

Based on the phase definitions proposed by Landlinger et al. (Landlinger et al., 2010) and adapted to the experimental setup of the present study, the forehand high-ball stroke was divided into three consecutive phases (Figure 2): backswing, forward swing, and follow-through.

The backswing phase extended from completion of the split step to the instant of maximum backswing, defined as the point at which the racket reached its most posterior position while shoulder external rotation and elbow flexion approached their maximum values. The forward swing phase extended from maximum backswing to the instant of initial racket–ball contact. The follow-through phase extended from ball contact to completion of the stroke, defined as the point at which racket motion reached the end of the swing trajectory and upper-limb motion had largely ceased. All phases were identified using kinematic events to ensure biomechanically meaningful and reproducible movement segmentation.

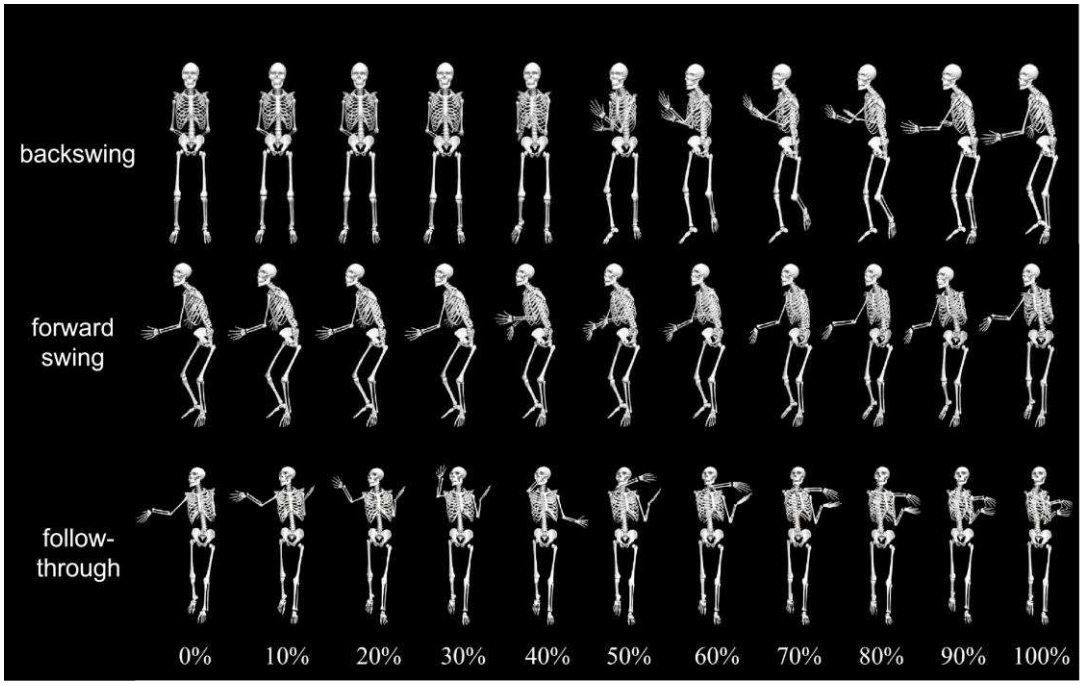


Figure 2. Temporal events and phase definition of the tennis forehand high-ball stroke.

1.3 Variables and data processing

1.3.1 Kinematic variables

Three-dimensional kinematic variables were extracted throughout the entire forehand high-ball stroke. Lower-limb variables included hip flexion/extension, abduction/adduction, and internal/external rotation; knee flexion/extension, varus/valgus, and internal/external rotation; and ankle dorsiflexion/plantarflexion, inversion/eversion, and internal/external rotation. Upper-limb variables comprised shoulder flexion/extension, abduction/adduction, and internal/external rotation, together with elbow flexion/extension, varus/valgus, and forearm pronation/supination. Pelvic anterior/posterior tilt, lateral tilt, and axial rotation, as well as thoracic flexion/extension, lateral flexion, and axial rotation, were also included in the analysis.

1.3.2 Data processing

Raw motion capture data were initially processed using Qualisys Track Manager (QTM; Qualisys AB, Gothenburg, Sweden) to reconstruct marker trajectories and define anatomical coordinate systems. The processed kinematic data were subsequently exported to Visual3D (C-Motion Inc., Germantown, MD, USA) for further analysis. Marker trajectories were filtered using a fourth-order zero-lag Butterworth low-pass filter with a cut-off frequency of 12 Hz (Lenz et al., 2021; Jolliffe and Cadima, 2016).

All kinematic waveforms were time-normalized to 101 data points (0–100%) for each movement phase (backswing, forward swing, and follow-through). Consequently, each participant was represented by 12,726 variables (42 kinematic variables × 303 normalized time points).

Prior to principal component analysis (PCA), all variables were standardized to z-scores to eliminate differences in measurement scale:

$$Z_{ij} = \frac{X_{ij} - \bar{X}_j}{S_j}$$

where X_{ij} denotes the value of variable j for participant i, $\bar{X}_j$ is the mean of variable j, and S_j is its standard deviation.

Principal component analysis was then performed on the standardized data matrix containing 28 participants and 12,726 kinematic variables. Principal components accounting for more than 80% of the cumulative variance were retained for subsequent

analyses(Li et al., 2016; Nishiyama, 2025). Each principal component represented a dominant movement pattern reflecting coordinated variations across multiple joints and body segments.

1.4 Statistical analysis

Statistical analyses were performed using IBM SPSS Statistics 27.0 (IBM Corp., Armonk, NY, USA). Normality was assessed using the Shapiro–Wilk test. Pearson correlation coefficients were calculated to examine the relationships between principal component scores (PCSs) and both peak racket-head speed and peak racket-head acceleration.

To facilitate biomechanical interpretation of each principal component, representative movement waveforms were reconstructed by perturbing the corresponding PCS by ±3 SD while all remaining principal components were maintained at their mean values (He et al., 2022). For principal components showing significant positive correlations with the performance variables, the +3 SD reconstruction represented the higher-performance condition, whereas the −3 SD reconstruction represented the lower-performance condition, thereby illustrating the movement characteristics associated with superior and inferior stroke performance.

2. Results

2.1 Racket-head speed and acceleration

The mean peak racket-head speed was 20.71 ± 2.25 $m \cdot s^{-1}$, ranging from 17.17 to 24.81 $m \cdot s^{-1}$. The mean peak racket-head acceleration was 437.14 ± 97.90 $m \cdot s^{-2}$, with values ranging from 297.75 to 611.12 $m \cdot s^{-2}$.

2.2 Principal component analysis and correlation analysis

The first 13 principal components explained 80.43% of the total kinematic variance (Table 2). Among these components, only the fifth principal component (PC5) was significantly correlated with both peak racket-head speed ($r = 0.553$, $p = 0.002$) and peak racket-head acceleration ($r = 0.485$, $p = 0.009$). Based on the PC5 loading matrix, variables contributing to the top 5% of the loading magnitude were identified as key features for subsequent waveform reconstruction.

Table 2. Variance explained by each principal component and correlations between principal component scores and peak racket-head speed and peak racket-head acceleration.

Principal component	Variance explained (%)	Cumulative variance (%)	Peak racket-head speed *r* (*p*)	Peak racket-head acceleration *r* (*p*)
PC1	13.40	13.40	−0.019 (0.925)	−0.051 (0.796)
PC2	10.47	23.87	−0.079 (0.688)	−0.011 (0.955)
PC3	9.01	32.88	0.263 (0.176)	0.162 (0.411)
PC4	7.23	40.11	0.111 (0.575)	0.013 (0.949)
PC5	**6.65**	**46.76**	**0.553 (0.002)**	**0.485 (0.009)**
PC6	6.25	53.01	−0.184 (0.348)	−0.239 (0.221)
PC7	5.16	58.17	−0.291 (0.133)	−0.287 (0.139)
PC8	4.70	62.86	0.035 (0.861)	0.121 (0.541)
PC9	4.48	67.34	−0.054 (0.786)	−0.019 (0.923)
PC10	4.26	71.60	−0.131 (0.507)	−0.009 (0.965)
PC11	3.19	74.80	0.140 (0.476)	0.078 (0.691)
PC12	2.98	77.78	−0.229 (0.240)	−0.158 (0.421)
PC13	2.65	80.43	0.151 (0.443)	0.142 (0.472)

PC, principal component; r, Pearson correlation coefficient; p, p-value.

2.3 Waveform reconstruction

Waveform reconstruction based on PC5 demonstrated the movement characteristics associated with peak racket-head speed and peak racket-head acceleration (Figures 3–5).

2.4 Backswing phase

During the backswing phase, waveform reconstruction identified pronounced differences between the reconstructed higher- and lower-performance waveforms in right hip abduction/adduction, left tibial internal/external rotation, left elbow varus/valgus, and thoracic axial rotation (Figure 3).

The reconstructed waveform for right hip abduction/adduction diverged primarily during the final 93–100% of the backswing (Figure 3a). The higher-performance waveform exhibited greater hip abduction, whereas the lower-performance waveform showed a slight tendency toward hip adduction.

For left tibial internal/external rotation, the principal differences occurred between 15% and 75% of the backswing (Figure 3b). The higher-performance waveform

remained close to the neutral position throughout this period, whereas the lower-performance waveform displayed greater external rotation.

Differences in left elbow varus/valgus were concentrated between 31% and 36% of the backswing (Figure 3c). Compared with the lower-performance waveform, the higher-performance waveform demonstrated a larger varus angle during this interval.

For thoracic axial rotation, the most influential region occurred during the initial 0–8% of the backswing (Figure 3d). Both reconstructed waveforms showed a progressive rotation toward the left; however, the higher-performance waveform exhibited an earlier onset and a greater magnitude of thoracic rotation.

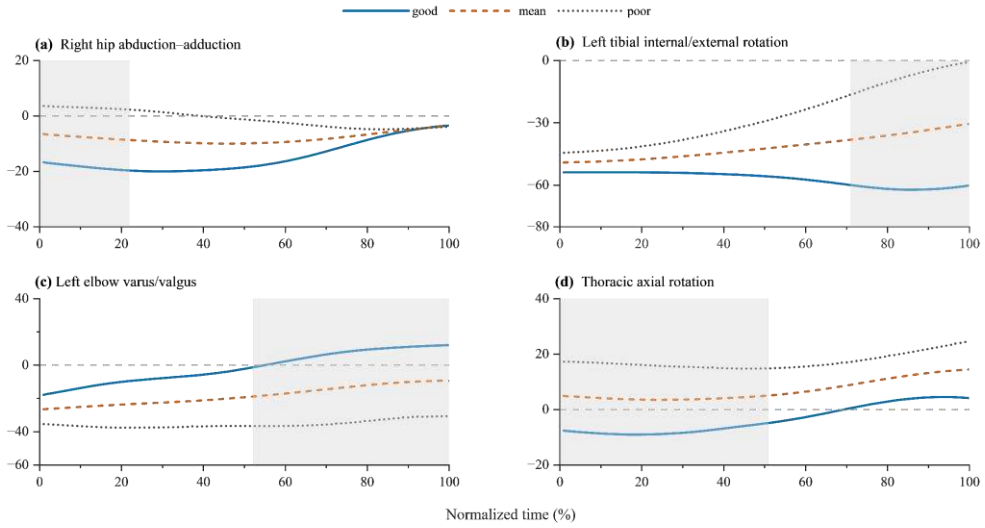


Figure 3. Waveform reconstruction of key kinematic variables during the backswing phase based on the fifth principal component (PC5).

Reconstructed joint angle waveforms for right hip abduction/adduction (a), left tibial internal/external rotation (b), left elbow varus/valgus (c), and thoracic axial rotation (d) are shown. Grey shaded regions indicate the high-loading intervals (top 5% of PC5 loading magnitudes), representing the portions of the movement that contributed most strongly to PC5.

2.5 Forward swing phase

During the forward swing phase, waveform reconstruction identified distinct differences between the reconstructed higher- and lower-performance waveforms in right hip abduction/adduction, right shoulder abduction/adduction, left knee varus/valgus, and left ankle inversion/eversion (Figure 4).

The reconstructed waveforms for right hip abduction/adduction diverged during the initial 0–21% of the forward swing (Figure 4a). The higher-performance waveform maintained a greater degree of hip abduction throughout this interval, whereas the

lower-performance waveform progressed from hip adduction toward a more neutral position.

Differences in right shoulder abduction/adduction were observed during the final 70–100% of the forward swing (Figure 4b). Compared with the lower-performance waveform, the higher-performance waveform demonstrated consistently greater shoulder abduction. In contrast, the lower-performance waveform showed a progressive reduction in shoulder abduction toward ball contact.

For left knee varus/valgus, the principal differences occurred between 51% and 100% of the forward swing (Figure 4c). The higher-performance waveform transitioned from slight valgus to a more pronounced varus alignment, whereas the lower-performance waveform remained predominantly in valgus throughout this interval.

Differences in left ankle inversion/eversion were concentrated during the initial 0–50% of the forward swing (Figure 4d). The higher-performance waveform remained in eversion with a gradual reduction in eversion angle, whereas the lower-performance waveform remained in inversion throughout the corresponding period.

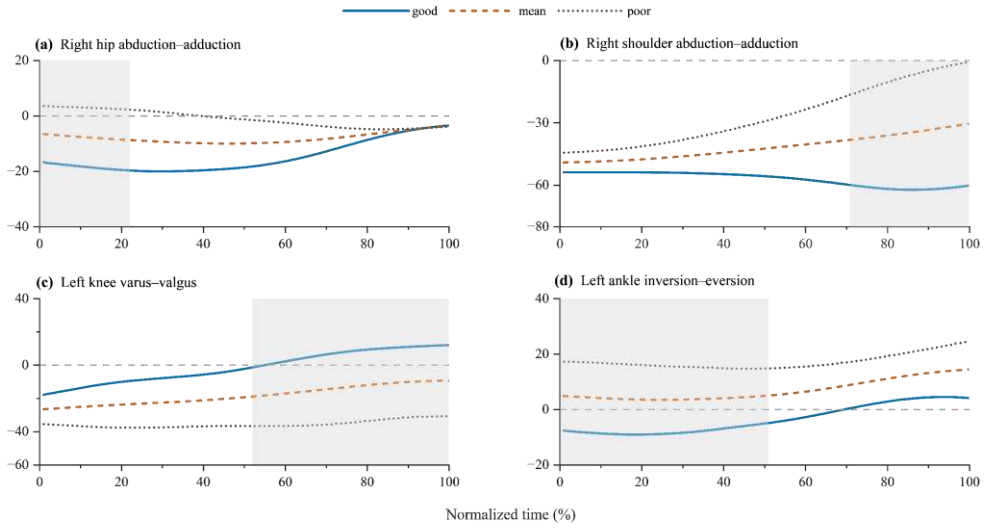


Figure 4. Waveform reconstruction of key kinematic variables during the forward swing phase based on the fifth principal component (PC5).

Reconstructed joint angle waveforms for right hip abduction/adduction (a), right shoulder abduction/adduction (b), left knee varus/valgus (c), and left ankle inversion/eversion (d) are shown. Grey shaded regions indicate the high-loading intervals (top 5% of PC5 loading magnitudes), representing the portions of the movement that contributed most strongly to PC5.

2.6 Follow-through phase

During the follow-through phase, waveform reconstruction identified distinct differences between the reconstructed higher- and lower-performance waveforms in right shoulder abduction/adduction, right elbow flexion/extension, pelvic obliquity, thoracic lateral flexion, thoracic axial rotation, left knee varus/valgus, and left ankle inversion/eversion (Figure 5).

Differences in right shoulder abduction/adduction were observed during the initial 0–17% of the follow-through (Figure 5a). The higher-performance waveform demonstrated greater shoulder abduction, followed by a gradual reduction toward a neutral position, whereas the lower-performance waveform remained close to neutral throughout this interval.

For right elbow flexion/extension, the principal differences occurred between 1% and 16% of the follow-through (Figure 5b). The higher-performance waveform exhibited a smaller elbow flexion angle and a brief extension before returning to flexion, whereas the lower-performance waveform showed a progressive increase in elbow flexion.

Differences in pelvic obliquity were identified during 41–100% of the follow-through (Figure 5c). The higher-performance waveform maintained a slight left-up/right-down pelvic orientation while gradually approaching a neutral position. In contrast, the lower-performance waveform displayed a right-up/left-down orientation with progressively greater pelvic obliquity.

For thoracic lateral flexion, the reconstructed waveforms diverged during 43–100% of the follow-through (Figure 5d). The higher-performance waveform remained in slight right lateral flexion and gradually returned toward neutral, whereas the lower-performance waveform demonstrated greater left lateral flexion throughout this interval.

During 78–100% of the follow-through, the lower-performance reconstruction showed a greater thoracic axial rotation angle than the higher-performance reconstruction, while both curves remained relatively stable (Figure 5e). Both reconstructed waveforms continued to rotate toward the left; however, the lower-performance waveform exhibited a greater magnitude of thoracic axial rotation.

For left knee varus/valgus, the principal differences occurred during the initial 0–15% of the follow-through (Figure 5f). The higher-performance waveform remained in

slight varus with a gradual reduction in varus angle, whereas the lower-performance waveform remained predominantly in valgus throughout this period.

Differences in left ankle inversion/eversion were observed between 8% and 71% of the follow-through (Figure 5g). Both reconstructed waveforms remained relatively stable; however, the lower-performance waveform exhibited greater ankle inversion, whereas the higher-performance waveform remained closer to a neutral ankle position.

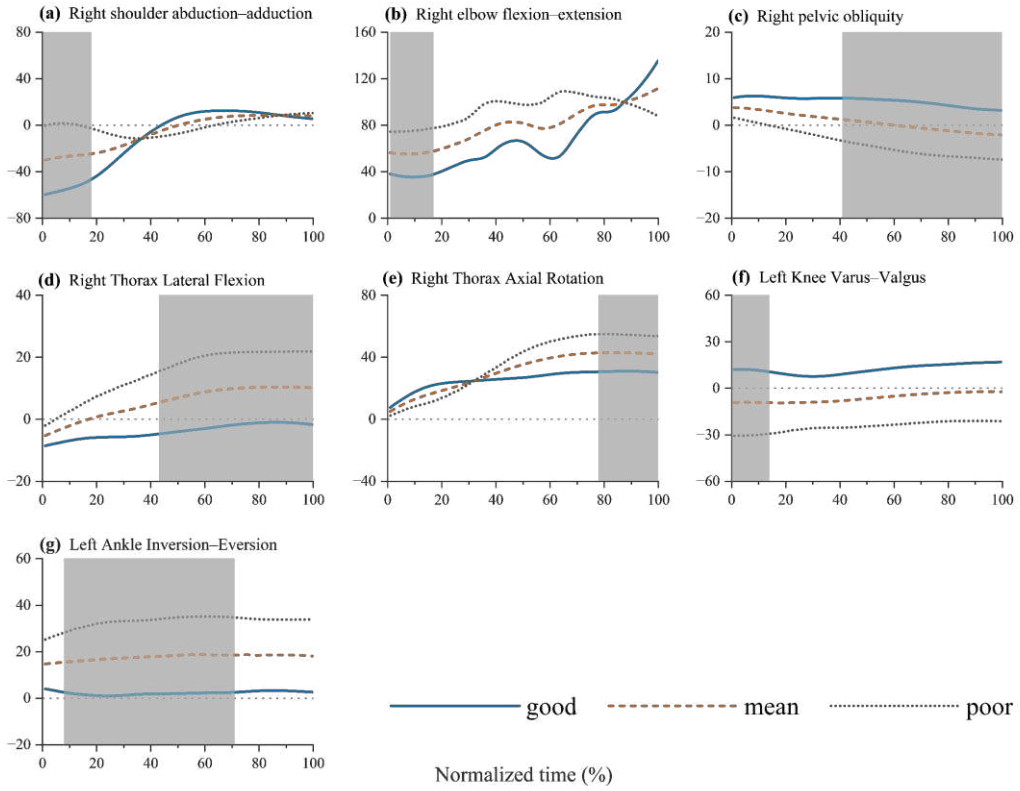


Figure 5. Waveform reconstruction of key kinematic variables during the follow-through phase based on the fifth principal component (PC5).

Reconstructed joint angle waveforms for right shoulder abduction/adduction (a), right elbow flexion/extension (b), pelvic obliquity (c), thoracic lateral flexion (d), thoracic axial rotation (e), left knee varus/valgus (f), and left ankle inversion/eversion (g) are shown. Grey shaded regions indicate the high-loading intervals (top 5% of PC5 loading magnitudes), representing the portions of the movement that contributed most strongly to PC5.

3. Discussion

The first 13 principal components explained 80.43% of kinematic variance, but only PC5 was significantly associated with both peak racket-head speed and acceleration. PCA captures the main sources of movement variability (Nishiyama,

2025), which need not be associated with performance. Most retained components showed no significant correlations with either outcome. PC5 may therefore distinguish aspects of movement organization relevant to racket performance from broader differences in individual movement style (Bernstein, 1967; Scholz and Schöner, 1999; Latash, 2012) Higher- and lower-performance patterns here refer to waveforms reconstructed at PC5 scores three standard deviations above and below the mean.

During the late backswing, the reconstructed higher-performance waveform showed greater right hip abduction. This position may provide a favorable base for subsequent pelvic and trunk rotation, consistent with the proposed contribution of hip alignment to stroke preparation (Huang and Gao, 2023; He et al., 2022). The left tibia also remained closer to neutral during 15–75% of the backswing, whereas the lower-performance waveform showed greater external rotation. Such alignment may reflect task-specific stabilization, in which limiting unnecessary motion supports the movement as a whole (Scholz and Schöner, 1999; Latash et al., 2007). The combination of these features may help preserve a stable lower-limb support structure during racket preparation.

The higher-performance waveform also showed greater left elbow varus during 31–36% of the backswing. This difference may reflect upper-limb positioning during racket preparation rather than greater joint mobility. Interactions between trunk and upper-limb motion provide a possible context for this finding (Hank et al., 2024; Mine et al., 2025), while the reconstructed pattern illustrates how joint posture can be considered within the overall movement (Federolf et al., 2014).

During the forward swing, differences in hip and shoulder positioning suggested a more open configuration in the higher-performance waveform. These observations are consistent with an emphasis on coordinated segmental motion in striking tasks (Zhang and Chen, 2024; Putnam, 1993). Greater right hip abduction persisted during 0–21% of this phase, whereas the lower-performance waveform moved from adduction toward neutral. Maintaining an abducted hip position may support pelvic stability and trunk rotation, given the hip's role in linking the lower limbs and trunk (Caprioli et al., 2025; Martin et al., 2020). Greater right shoulder abduction was apparent during 70–100% of the forward swing. The higher-performance waveform maintained this position closer to contact, whereas the lower-performance waveform showed earlier closing of the upper limb. This difference may reflect the relationship between shoulder

positioning and proximal segment coordination (Hank et al., 2024; Mine et al., 2025; Wen and Wang, 2025). The left knee and ankle also showed more continuous adjustments in the higher-performance waveform. These joints provide support while regulating posture, and their changing alignment may help accommodate the rotating upper body (Horak and Macpherson, 1996).

The observed differences concerned the timing and progression of joint motion as well as angular magnitude. Interpreting the waveforms together therefore provides information that isolated joint measures may miss. This perspective is consistent with the emphasis on whole-body coordination in related racket-sport research (Zhu et al., 2023).

The pelvis and thorax also remained closer to stable alignment in the higher-performance waveform, whereas the lower-performance waveform showed greater lateral deviation. Given the trunk's contribution to upper-body movement and its relationship with shoulder kinematics, these differences may indicate distinct strategies for recovering posture after contact (van Trigt et al., 2025; Mine et al., 2025). A steadier trunk position may reduce the need for postural corrections as the stroke ends. Thoracic rotation in the higher-performance waveform largely occurred early in follow-through before leveling off; the lower-performance waveform continued rotating through approximately the first 60%. This contrast suggests that rotational timing deserves consideration alongside rotation magnitude (Zhang and Chen, 2024; Li et al., 2016).

Taken together, PC5 linked racket performance with differences in movement timing, hip positioning, limb alignment, and trunk motion. These features are compatible with accounts of skill that emphasize the organization of available degrees of freedom (Bernstein, 1967; Latash, 2023). Earlier thoracic rotation and more stable alignment may be useful features to examine within coordinated stroke mechanics (van Trigt et al., 2025). For coaching, the findings support considering joint movements as parts of the complete stroke rather than prescribing larger excursions in isolation (Federolf et al., 2014). Whether training these features improves performance requires direct testing.

4. Conclusion

The present study identified PC5 as the principal movement pattern associated

with peak racket-head speed and peak racket-head acceleration during the tennis forehand high-ball stroke. This movement pattern was characterized by earlier thoracic rotation during the backswing, more favorable hip positioning and lower-limb alignment, maintenance of an open shoulder configuration during the forward swing, and more stable pelvic and thoracic control during the follow-through.

The association between PC5 scores and peak racket-head speed and acceleration suggests that whole-body movement organization is relevant to racket kinematic performance during the tennis forehand high-ball stroke. From a practical perspective, interventions targeting earlier trunk rotation and improved hip positioning during the backswing may promote more effective coordination of the upper limb during the forward swing, providing a biomechanical basis for technique refinement and performance enhancement in tennis.

Declarations

Ethics approval and consent to participate

This study was approved by the Medical Ethics Committee of Qinhuangdao Hospital, Peking University Third Hospital (Approval No. 2026Y005). Written informed consent to participate was obtained from all participants before data collection.

Clinical trial number: not applicable.

Consent for publication

Written informed consent for publication of the photographs in Figure 1 was obtained from all individuals depicted.

Funding

No funding was received.

Competing interests

The authors declare no competing interests.

Availability of data and materials

The authors confirm that the data supporting the findings of this study are available in the supplementary materials accompanying this article.

Acknowledgements

Not applicable.

References

Huang T, Gao J. A Technical Study of Tennis Forehand Topspin Based on Sports Mechanics[J]. EAI Endorsed Transactions on Scalable Information Systems, 2023, 10(4): e9.

Lambrich J, Muehlbauer T. The role of increased post-impact ball speed on plantar pressure during topspin and slice longline forehand groundstrokes in female tennis players[J]. BMC Research Notes, 2023, 16(1): 330.

Genevois C, Reid M, Creveaux T, et al. Kinematic differences in upper limb joints between flat and topspin forehand drives in competitive male tennis players[J]. Sports biomechanics, 2020, 19(2): 212-226.

Biber S W, Champneys A R, Szalai R. Analysis of point-contact models of the bounce of a hard spinning ball on a compliant frictional surface[J]. IMA journal of applied mathematics, 2023, 88(3): 498-523.

Caprioli L, Campoli F, Romagnoli C, et al. Three Reasons for Playing the Tennis Forehand in Square Stance[J]. Journal of Functional Morphology and Kinesiology, 2025, 10(2): 215.

Elliott B, Reid M, Crespo M. Technique development in tennis stroke production[M]. International Tennis Federation, 2009.

Martin C, Sorel A, Touzard P, et al. Can the open stance forehand increase the risk of hip injuries in tennis players?[J]. Orthopaedic journal of sports medicine, 2020, 8(12): 2325967120966297.

van Trigt B, Faneker E, Leenen A J R, et al. Uncovering the hidden mechanics of upper body rotations in tennis serves using wearable sensors on Dutch professional players[J]. Frontiers in Sports and Active Living, 2025, 6: 1463299.

Gorce P, Jacquier-Bret J. Are there kinematic and kinetic parameters correlated with racket velocity during the tennis serve? A preliminary comparison between a slow and a fast serve for performance improvement[J]. Frontiers in Sports and Active Living, 2024, 6: 1451174.

Federolf P A. A novel approach to study human posture control: “Principal movements” obtained from a principal component analysis of kinematic marker data[J]. Journal of biomechanics, 2016, 49(3): 364-370.

Gløersen Ø, Myklebust H, Hallén J, et al. Technique analysis in elite athletes using principal component analysis[J]. Journal of sports sciences, 2018, 36(2): 229-237.

Deluzio K J, Astephen J L. Biomechanical features of gait waveform data associated with knee osteoarthritis: an application of principal component analysis[J]. Gait & posture, 2007, 25(1): 86-93.

Cappozzo A, Catani F, Della Croce U, et al. Position and orientation in space of bones during movement: anatomical frame definition and determination[J]. Clinical biomechanics, 1995, 10(4): 171-178.

Landlinger J, Lindinger S, Stöggl T, et al. Key factors and timing patterns in the tennis forehand of different skill levels[J]. Journal of sports science & medicine, 2010, 9(4): 643.

Lenz A L, Strobel M A, Anderson A M, et al. Assignment of local coordinate systems and methods to calculate tibiotalar and subtalar kinematics: A systematic review[J]. Journal of biomechanics, 2021, 120: 110344.

Jolliffe I T, Cadima J. Principal component analysis: a review and recent developments[J]. Philosophical transactions of the royal society A: Mathematical, Physical and Engineering Sciences, 2016, 374(2065): 20150202.

Li Z, Zhang W, Pan D, et al. Power calculation of multi-step combined principal components with applications to genetic association studies[J]. Scientific Reports, 2016, 6(1): 26243.

Nishiyama K. Identifying influential motion patterns in javelin throwing using principal component analysis[J]. Journal of Sports Sciences, 2025, 43(22): 2718-2730.

He Y, Fekete G, Sun D, et al. Lower limb biomechanics during the topspin forehand in table tennis: a systemic review[J]. Bioengineering, 2022, 9(8): 336.

Bernstein NA. The co-ordination and regulation of movements. Oxford: Pergamon Press; 1967.

Scholz J P, Schöner G. The uncontrolled manifold concept: identifying control variables for a functional task[J]. Experimental brain research, 1999, 126(3): 289-306.

Latash M L. The bliss (not the problem) of motor abundance (not redundancy)[J]. Experimental brain research, 2012, 217(1): 1-5.

Federolf P, Reid R, Gilgien M, et al. The application of principal component

analysis to quantify technique in sports[J]. Scandinavian journal of medicine & science in sports, 2014, 24(3): 491-499.

Elliott B. Biomechanics and tennis[J]. British journal of sports medicine, 2006, 40(5): 392-396.

Latash M L, Scholz J P, Schöner G. Toward a new theory of motor synergies[J]. Motor control, 2007, 11(3): 276-308.

Hank M, Miratsky P, Ford K R, et al. Exploring the interplay of trunk and shoulder rotation strength: a cross-sport analysis[J]. Frontiers in physiology, 2024, 15: 1371134.

Mine K, Jones M, Saunders S, et al. Relationships between upper trunk rotation kinematics and arm fatigue after repetitive pitching among baseball pitchers[J]. Sports Biomechanics, 2025, 24(7): 2134-2147.

Zhang Y, Chen Z. Kinematic differences in forehand serve-receiving techniques of the male tennis players at low and high-speed serves[J]. Scientific Reports, 2024, 14(1): 26586.

Putnam C A. Sequential motions of body segments in striking and throwing skills: descriptions and explanations[J]. Journal of biomechanics, 1993, 26: 125-135.

Wen S, Wang Q. Biomechanical model of forehand stroke of tennis players[J]. Molecular & Cellular Biomechanics, 2025, 22(5).

Horak F B, Macpherson J M. Postural orientation and equilibrium[J]. Comprehensive physiology, 1996: 255-292.

Zhu R, Yang X, Chong L C, et al. Biomechanics of topspin forehand loop in table tennis: an application of opensim musculoskeletal modelling[C]//Healthcare. MDPI, 2023, 11(9): 1216.

Latash M L. The control and perception of antagonist muscle action[J]. Experimental Brain Research, 2023, 241(1): 1-12.

Supplementary Files

This is a list of supplementary files associated with this preprint. Click to download.

- date.zip